Solar World Congress 2025

SOL-GEL COBALT-FREE SPINEL OXIDE AS A SELECTIVE SOLAR ABSORBER: ACHIEVING HIGH EFFICIENCY WITHOUT CRITICAL RAW MATERIALS

Federico Turci[1], Andreas Schüler[1]

1 EPFL, Laboratory of Nanotechnology for Solar Energy Conversion, Lausanne (Switzerland)

Abstract

This study develops a cobalt-free $CuMnO_x$ multilayer solar absorber to replace $CuMnCoO_4$, which offers ~0.95 solar absorption and ~0.15 emissivity. Driven by cobalt's environmental and supply risks, we optimized dip-coating parameters and layer thicknesses on stainless steel using ellipsometry, simulations, and experimental validation. Spectroscopic ellipsometry revealed that cobalt mainly affects the extinction coefficient (k) in the visible range, enhancing absorption via electronic transitions, while its impact in the silica-spinel layer is negligible. The cobalt-free $CuMnO_x$ showed slower k decay in the near-infrared (1.5-2.0 μm), explaining its higher absorption in this range. Transfer-matrix modeling (TFCalc) predicted an optimal multilayer design with a theoretical α_{sol} of 0.957, closely matched by the measured performance. The empirical correlation between film thickness and withdrawal speed exhibited a regime shift at 7 mm/s, consistent with Landau-Levich and gravitational-viscous deposition regimes. Morphological analyses confirmed nanocrystallinity and superior homogeneity for the cobalt-free coating, leading to enhanced reproducibility and scalability. Overall, the cobalt-free $CuMnO_x/CuMnSiO_x/SiO_2$ multilayer exhibits comparable optical performance to its cobalt-containing counterpart, validating it as a sustainable and industrially viable alternative for solar thermal absorbers.

Keywords: $CuMnO_x$, Selective solar absorber, Cobalt-free, Sol-gel, Dip-coating, Ellipsometry

1. Introduction

Solar thermal systems rely on selective absorber coatings that maximize solar absorption and minimize heat losses. These materials are key components in a wide range of applications, including Concentrated Solar Power (CSP), industrial process heating, and domestic hot water production. Spinel oxides like $CuMnCoO_4$ offer excellent optical selectivity, thermal stability, and high solar absorptance, making them ideal for these applications [1], [2], [3], [4], [5]. However, cobalt is a critical raw material with supply chain concerns, motivating the search for cobalt-free alternatives [6], [7]. Previous studies have shown that some cobalt-free absorbers can achieve favorable optical properties and durability[8], especially when deposited on aluminum substrates, using either aqueous or ethanol-based solutions [2], [9], [10], [11]. Nonetheless, aluminum is representative of substrates used in flat plate collectors, but not for concentrated applications, where stainless steel tubes are preferred due to their superior mechanical stability, resistance to corrosion, efficient heat transfer, and suitability for food-grade applications [12], [13]. Coating stainless steel is challenging due to its surface roughness, limited adhesion, and complex alloy composition. The presence of multiple alloying elements, added to enhance corrosion resistance, can lead to unpredictable reactions during heat treatments. [14], [15]. The present study explores whether good performances can be obtained with cobalt-free absorbers on stainless steel substrates. A comparison between a multilayer composed by $CuMnCoO_4$ and one composed by $CuMnO_x$ was investigated; both cobalt-containing and cobalt-free triple-layer absorbers feature a graded-index structure: a base layer for strong absorption ($CuMnO_x$ or $CuCoMnO_x$), a middle layer composed of a spinel-silica nanocomposite to provide a refractive index transition ($CuMnSiO_x$ or $CuCoMnSiO_x$), and a SiO_2 top layer for anti-reflection. Increasing the silicon content lowers both n and k, enhancing spectral selectivity and providing wavelength-selective properties. Notably, the extinction coefficient k decreases with increasing wavelength, making these materials suitable selective solar absorbers. Maintaining a moderate refractive index

10.18086/swc.2025.01.22 Available at http://proceedings.ises.org

n also helps minimize strong surface and interface reflections[16], [17], [18] The target performance for these coatings is high solar absorptance (>0.94) across the 0.4–2.5 µm solar spectrum while keeping thermal emittance below 0.20 in the mid-infrared range, enabling efficient operation in concentrated solar systems [19], [20].

2. Experimental section

2.1 *Solutions*

All precursor solutions were formulated based on the methodology outlined by Joly et.al [3], and detailed below. The Cu-Co-Mn formulation was derived using manganese (II) acetate tetrahydrate (99\%, Fisher Scientific), copper (II) chloride dihydrate (99\%, Fisher Scientific), and cobalt (II) chloride hexahydrate (98\%, Fisher Scientific). Initially, manganese acetate was dissolved in nitric acid (HNO_3). Subsequently, absolute ethanol, cobalt chloride, copper chloride, demineralized water, and PEG200 were incrementally incorporated into the mixture. Using a rotary evaporator (Büchi Rotavapor R-210), over 95 wt\% of ethanol was removed by evaporation (70°C, 200 mbar) to concentrate the precursor species. Fresh absolute ethanol was then reintroduced to restore the initial molar concentration. This process aimed to enhance the hydrolysis and condensation mechanisms within the solution [21]. A surfactant (Triton-X100) was subsequently incorporated, and the solution was kept at 70~°C for 15~hours before being used for dip-coating. A separate solution for SiO_x layer deposition was prepared using tetraethyl-orthosilicate (TEOS, 98\%, Acros). TEOS was added to absolute ethanol and hydrolyzed in the presence of nitric acid and demineralized water. After aging at 50°C for 15 hours, the solution was ready for use in dip-coating. The final Cu-Co-Mn-Si solution was obtained by blending the two previously prepared solutions. The selected molar proportions of Cu-Co-Mn-Si for the three formulations were based on previous studies[1], [22] and correspond to (1:1:1: 0), (1:1:1:1), and (0:0:0:1). The cobalt-free precursor solution was prepared using the same reagents and following the same steps, maintaining the same stoichiometric ratio between metals and silicon in the three layers: Cu-Mn-Si (1:1:0), (1:1:1), and (0:0:1).

2.2 Deposition

To ensure the formation of uniform, particle-free coatings, a custom-built setup was designed in the laboratory and previously described in the literature [23], [24]. The dip-coating withdrawal speed was selected based on empirical calibration curves, showed in the result section. Following each dip-coating step, the samples were placed in a Vulcans benchtop furnace at room temperature. The temperature was increased at 30 °C per minute to 400 °C, for the cobalt-containing coatings, and to 500°C for cobalt-free coatings. The films were then subjected to a thermal treatment at the maximum temperature for 90 minutes, followed by natural cooling inside the furnace. All sample depositions were carried out under a laminar flow hood equipped with an Arida Pro S19 dehumidifier, which includes an integrated controller for both relative humidity and temperature, ensuring stable environmental conditions during the process. All depositions were conducted at a constant temperature of 25°C.

2.3 Substrate

The multilayer solar absorber was deposited on silica wafers (001), used as received, and on polished austenitic stainless steel (1.4301) with typical dimensions of 7 x 6 cm. The roughness of this substrate was previously measured using atomic force microscopy (AFM, Solver Pro-M from NT-MDT), yielding a root mean square value of 28 nm. Samples were cleaned via a sonic bath, first in acetone, then ethanol, each for 5 minutes, and finally rinsed with hot demineralized water.

2.4 Optical properties

Reflectance was measured from 0.4–14 µm: in the 0.4–2.5 µm range using an Oriel MultiSpec 125™ and Cary 5 spectrophotometer with an integrating sphere; and from 2.5–14 µm with a Varian 3100 FT-IR. Solar absorptance (α_{sol}) was calculated using the solar irradiance spectrum (reference spectrum: ASTM G173-03 DC) (eq. 1):

$$\alpha_{sol} = \frac{\int_{0.4}^{2.5} I_{sol}(\lambda)(1-\rho(\lambda))d\lambda}{\int_{0.4}^{2.5} I_{sol}(\lambda)d\lambda} \quad \text{(eq. 1)}$$

Where $\rho(\lambda)$ is the spectral reflectivity and I_{sol} is the solar irradiance on the ground. In the thermal-infrared region, the spectral emissivity for opaque materials can be expressed in terms of total spectral reflectance using Kirchhoff's law [25] (eq. 2):

$$\varepsilon(\lambda) = \alpha(\lambda) = 1 - \rho(\lambda) \quad \text{(eq. 2)}$$

where $\varepsilon(\lambda)$ is the spectral emissivity, $\alpha(\lambda)$ the spectral absorptivity. By weighting the total spectral emissivity (measured over the 2.5 – 14 μm spectral range) with the black body radiation of a body at T = 373 ° K, the thermal emittance of the absorber, ε_{th} is determined:

$$\varepsilon_{th} = \frac{\int_{2.5}^{14} \varepsilon(\lambda)E_b(\lambda,T)d\lambda}{\int_{2.5}^{14} E_b(\lambda,T)d\lambda} \quad \text{(eq. 3)}$$

Where E_b is the blackbody radiation at the given temperature. Spectroscopic ellipsometry (SE) measures changes in the polarization state of an incidence light beam after it is reflected off a sample [26] With the use of a physical model it's possible to extract information like refractive index, film thickness and porosity[27], [28]. A Woolam RC2 ellipsometer was employed to measure the ellipsometric angles Ψ and Δ, across the spectral range of wavelengths from 0.25 μm to 2.5 μm at incident angles of reflection ranging from 60° to 75°. To extrapolate n and k values we employed a Tauc-Lorentz model for the first layer and Tauc-Lorentz with Maxwell-Garnett Effective Medium Approximation (EMA) for the second layer for both cobalt-containing and cobalt-free formulations [29], [30]. $CuMnO_x$ and $CuMnSiO_x$ optical constant were used in TFCalc software to simulate the optimal thickness combination for the different layers, then used as a guide for the empirical test. Optimal thicknesses for the cobalt-containing absorber were already assessed in previous publications[16] TFCalc applies the transfer-matrix method based on Fresnel equation (eq. 4) to compute the optical response of multilayer stacks from optical constants and layer thicknesses. The equation is:

$$\rho(\lambda) = \left|\frac{(n(\lambda)-1)^2+k(\lambda)^2}{(n(\lambda)+1)^2+k(\lambda)^2}\right| \quad \text{(eq. 4)}$$

where total reflectance $\rho(\lambda)$, n is the real part of the refractive index and k is the extinction coefficient. This relationship allows correlating the optical constants obtained from ellipsometry with the experimentally measured reflectance spectra and transfer-matrix simulations, clarifying how variations in n and k influence the absorption behavior of the coatings [28].

2.5 Morphology

Scanning electron microscopy using the Zeiss Gemini SEM 300 was employed to investigate morphology of the films.

3. Results

The investigation aimed to determine whether a multilayer based on a cobalt-free black oxide material and a silicon nanocomposite could achieve high solar absorption and low thermal emissivity when deposited on a stainless-steel substrate. The first step involved measuring the optical constants of both cobalt-free and cobalt-containing coatings via spectroscopic ellipsometry. Figure 1 shows *n* and *k* for the first and second layers of both materials. Optical constants for the third, antireflective layer, were taken from the EASE software library, as it is a well-known material. Notably, the cobalt-free material exhibits a lower refractive index in the visible range but higher extinction coefficient compared to the cobalt-containing coating, suggesting a potential reduction in visible absorption but increased near-infrared (NIR) absorption.

Using the measured optical constants transfer-matrix simulations (TFCalc) were performed to simulate the spectral reflectance of the optimal multilayer cobalt-free absorber layout; the best result obtained is shown in Figure 2. These simulations served as a guide for the empirical investigation correlating withdrawal speed and layer thickness. The empirical study is shown in Figure 3, layers thicknesses were estimated through ellipsometry. In order to find the best combinations of film dimensions, the best performing $CuMnO_x$ layer was selected and kept constant for the multilayer layout exploration. After deposition of the selected thickness combinations, total reflectance was measured, and solar absorptance and thermal emissivity were calculated. Table 1 reports the performance obtained for the different combinations and Figure 4 presents the spectra of the sample exhibiting the best performance in both the visible–NIR and far IR regions. Figure 5a-b shows the SEM morphology investigations, comparing cobalt-free and cobalt-containing first two layers.

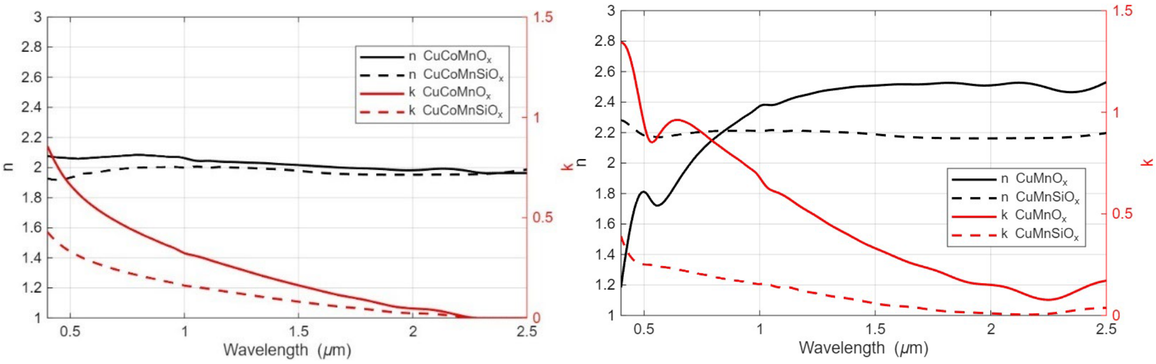

Figure 1. Refractive index (n) and extinction coefficient (k) of the first ($CuMnO_x$ and $CuMnCoO_x$) and second ($CuMnSiO_x$ and $CuMnCoSiO_x$) layers extracted from spectroscopic ellipsometry. The k values of $CuMnO_x$ in the visible region indicate that substantial absorption is maintained even in the absence of cobalt. $CuMnSiO_x$ and $CuMnCoSiO_x$ exhibit intermediate optical constants, consistent with their function as graded-index layers.

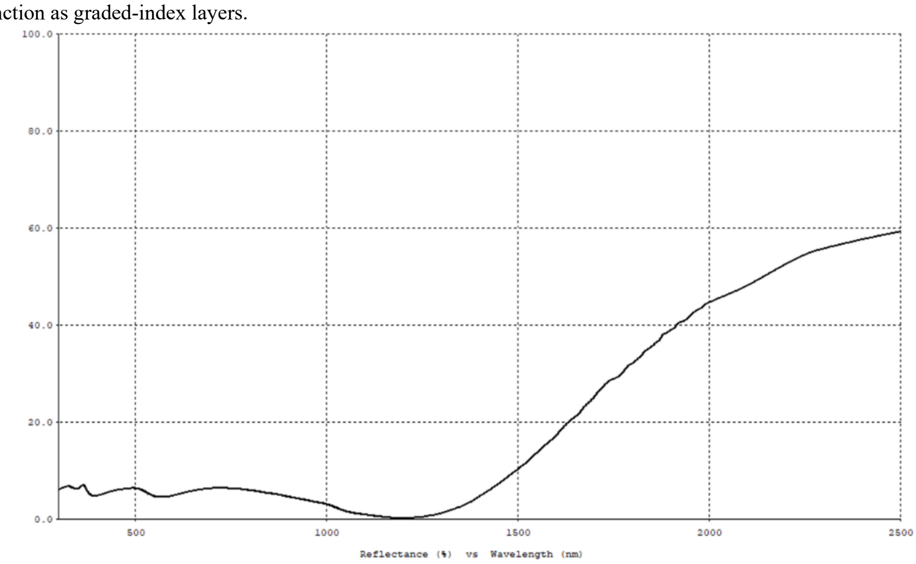

Figure 2. Simulated spectral reflectance of the $CuMnO_x/CuMnSiO_x/SiO_2$ multilayer absorber calculated using TFCalc. The simulation was based on the measured optical constants and indicates the theoretical performance of the multilayer. Optimal layer thicknesses predicted for maximum solar absorption were 80 nm, 60 nm, and 50 nm for the first, second, and third layers, respectively. The corresponding solar absorptance (α_{sol}) calculated from this simulated spectrum is 0.957, demonstrating the potential efficiency of the cobalt-free multilayer configuration.

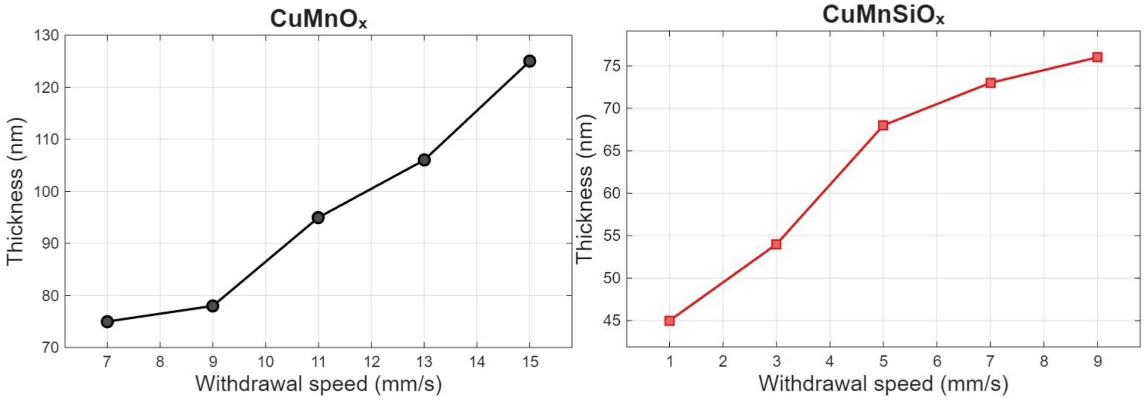

Figure 3. Empirical correlation between layer thickness and withdrawal speed for the first two layers of the multilayer absorbers: (a) $CuMnO_x/CuMnSiO_x$ and (b) $CuMnCoO_x/CuMnCoSiO_x$. These plots were used to determine the optimal deposition speeds to achieve the target thicknesses predicted by TFCalc simulations, guiding the experimental fabrication of the multilayers to closely reproduce the theoretical spectral performance.

$CuMnO_x$ (mm/s)	α_{sol}	$CuMnO_x$ (mm/s)	$CuMnO_x$ (mm/s)	SiO_2 (mm/s)	α_{sol}
7	0.8459	8	3	1,5	0.9324
8	0.8510	8	3	5	0.9284
9	0.8421	8	5	1.5	0.9358
10	0.8455	8	5	5	0.9549
11	0.8427	8	7	1.5	0.9350
12	0.8439	8	7	5	0.9253

Table 1. The table reports α_{sol} values for variations of the first $CuMnO_x$ layer, followed by the combinations of withdrawal speeds tested for the second $CuMnSiO_x$ layer while keeping the first layer fixed, and finally the top SiO_2 layer. These data identify the set of deposition speeds that yielded the multilayer sample with the highest overall solar absorptance.

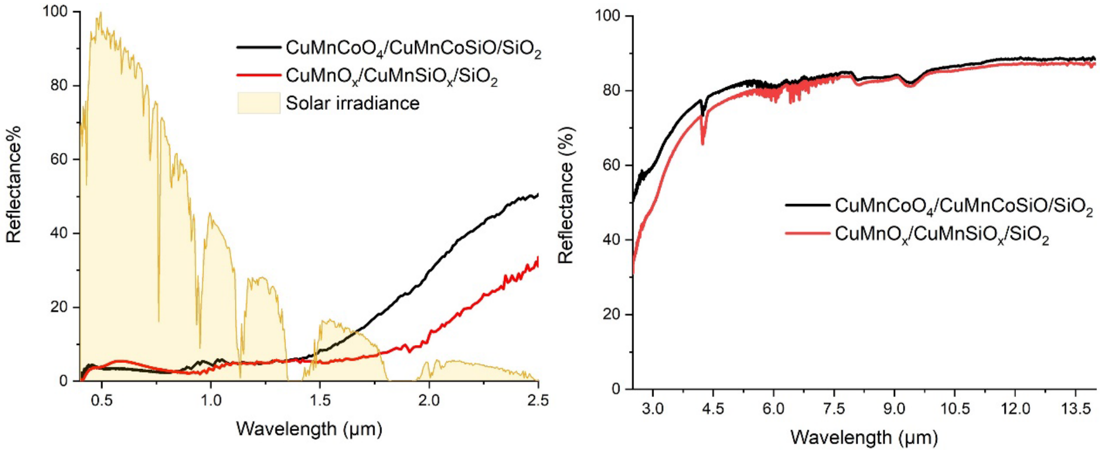

Figure 4: Total reflectance of both cobalt-containing and cobalt-free triple-layer absorbers was measured and compared with ground-level solar irradiance to evaluate absorptance and emittance. The cobalt-free absorber shows a reflectance minimum shift from ~0.8 µm to ~0.95 µm. In the visible range, cobalt-based coatings reflect less, indicating higher absorption. Between 1.4–1.8 µm, the cobalt-free variant reflects less. In the far-infrared, the cobalt-containing sample has slightly higher reflectance, implying lower emittance

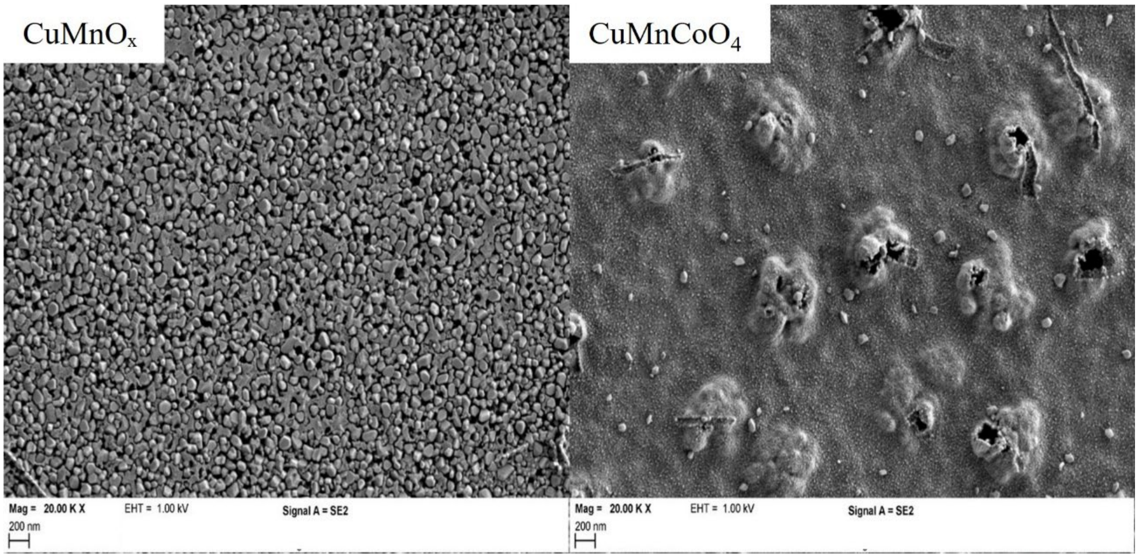

Figure 5a: SEM images show that $CuMnO_x$ has a uniform, nanocrystalline structure with consistent thickness and no major defects. In contrast, $CuMnCoO_4$ displays greater roughness and inhomogeneities, indicating less uniform deposition.

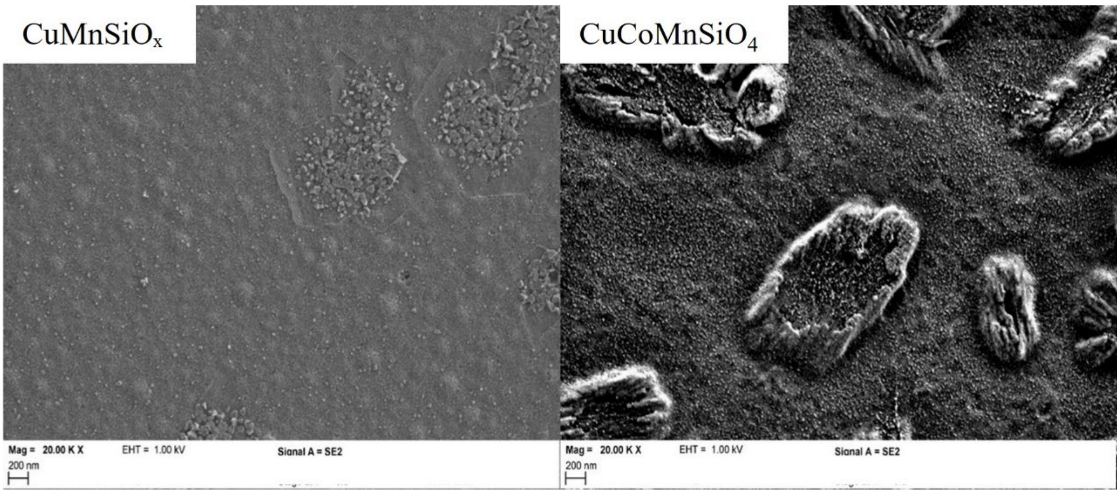

Figure 5b: SEM images compare cobalt-free and cobalt-containing second-layer nanocomposite coatings. The cobalt-containing layer shows thick, recurrent structures, leading to inhomogeneous thickness and reduced crystal purity, while the cobalt-free coating is homogeneous and defect-free.

4. Discussion and Conclusions

Reflectance measurements confirm strong solar absorption in the cobalt-free $CuMnO_x/CuMnSiO_x/SiO_2$ configuration on stainless steel. $CuMnO_x$ shows slightly higher solar absorptance (0.9549 ± 0.0027. Standard deviation obtained by 5 samples) compared to $CuMnCoO_4$ (0.9501 ± 0.0025. Standard deviation obtained by 5 samples), due to its better performance in the 1.4–2.0 µm range. Thermal emittance is slightly higher for the cobalt-free material (0.1694 ± 0.0022 vs. 0.1576 ± 0.0038), but this increase is minor compared to the absorption benefits. The behavior of the optical constants provides a clear rationale for the distinct reflectance trends observed between the two materials and elucidates the role of cobalt within the absorber. In the visible region (around 0.4 µm), the cobalt-free CuMnOx exhibits a relatively low refractive index ($n \approx 1.2$–1.5) but a high extinction coefficient ($k \approx 1.25$). While a low refractive index generally reduces Fresnel reflection, the simultaneous presence of a large k increases the numerator of the reflectance term, thereby enhancing ρ. This elevated k in the visible range accounts for the reflectance increase observed for the cobalt-free coating, whereas the cobalt-containing material, with its lower k, shows reduced reflectance and consequently higher absorption in this region, confirming the optical contribution of cobalt to visible light absorption. In the near-infrared range, the extinction coefficient of $CuMnO_x$ decreases slower than that of $CuCoMnO_x$, leading to substantially lower reflectance (≈10% vs. ≈30% between 1.5 and 2.0 µm). Optical constants extracted for the second layer, namely $CuMnSiO_x$ and $CuMnCoSiO_x$, were found to be very similar within experimental uncertainty. This close correspondence can be attributed to the nanocomposite character of the silica–spinel layer, in which the incorporation of SiO_2, characterized by its low refractive index and negligible absorption, effectively attenuates the optical influence of cobalt, rendering its contribution marginal in the overall optical response of the layer. These results indicate that cobalt exerts a dominant influence primarily in the first absorbing layer, where its electronic transitions directly affect visible absorption, whereas its impact within the silica-spinel layer is optically negligible. TFCalc simulations provided an initial estimation of the optimal layer thickness combination, predicting a theoretical solar absorptance of 0.957. The experimental reflectance closely reproduces the simulated trend, confirming the reliability of the Tauc-Lorentz model used to extract the optical properties of the oxide layers. The empirical correlation between film thickness and withdrawal speed revealed a change of regime occurring around 7 mm/s. For speeds below this threshold, the thickness follows a power-law dependence with an exponent of 2/3, consistent with the Landau–Levich regime, where viscous and surface tension forces are balanced. At higher speeds (above 7 mm/s), the relationship follows a power-law with an exponent of 1/2, indicating a transition to a regime dominated by viscous and gravitational forces. Morphological analysis revealed nanocrystallinity in the deposited coatings, with the cobalt-free material exhibiting higher homogeneity and better morphological control, suggesting less sensitivity to deposition conditions. In particular, the cobalt-free formulation produced smoother and more uniform grains across both the absorber and intermediate layers, while the cobalt-containing coating displayed larger and more irregular crystallites, with the presence of agglomerated structures of variable thicknesses, indicating a stronger dependence on drying kinetics. Since homogeneity and thickness control are crucial for industrial dip-coating methods, these findings support the conclusion that the cobalt-free alternative offers a more reliable and scalable solution for selective absorber production. Given its improved morphological and optical properties, as well as the elimination of cobalt, a critical raw material, this material presents a valuable alternative for large-scale manufacturing on stainless steel substrates. Although these findings, durability under thermal aging and environmental exposure remains to be verified. Furthermore, optimization and scaling up of the deposition parameters will be necessary to ensure reproducibility and cost effectiveness at industrial scale.

[1] L. Kalu$ Z Za, B. Orel, G. Dra$ Z Zi$ C C B, and M. Kohl, “Sol-gel derived CuCoMnO x spinel coatings for solar absorbers: Structural and optical properties,” 2001.

[2] R. Bayón, G. San Vicente, and Á. Morales, “Durability tests and up-scaling of selective absorbers based on copper–manganese oxide deposited by dip-coating,” *Solar Energy Materials and Solar Cells*, vol. 94, no. 6, pp. 998–1004, Jun. 2010, doi: 10.1016/j.solmat.2010.02.006.

[3] M. Joly *et al.*, “Optical and structural analysis of sol-gel derived Cu-Co-Mn-Si oxides for black selective solar nanocomposite multilayered coatings,” *Solar Energy Materials and Solar Cells*, vol. 143, pp. 573–580, 2015, doi: 10.1016/j.solmat.2015.06.058.

[4] A. Krammer, M. Lagier, and A. Schüler, "In-line electronic and structural characterization of reactively sputtered Cu-Co-Mn black spinel oxides," *Journal of Vacuum Science & Technology A: Vacuum, Surfaces, and Films*, vol. 39, no. 5, Sep. 2021, doi: 10.1116/6.0001120.

[5] E. B. Rubin, Y. Chen, and R. Chen, "Optical properties and thermal stability of Cu spinel oxide nanoparticle solar absorber coatings," *Solar Energy Materials and Solar Cells*, vol. 195, pp. 81–88, Jun. 2019, doi: 10.1016/j.solmat.2019.02.032.

[6] S. H. Farjana, N. Huda, and M. A. P. Mahmud, "Life cycle assessment of cobalt extraction process," *Journal of Sustainable Mining*, vol. 18, no. 3, pp. 150–161, Aug. 2019, doi: 10.1016/j.jsm.2019.03.002.

[7] "DGT thresholds adaptation Cobalt-copper-manganese-zinc."

[8] D. E. Karas, J. Byun, J. Moon, and C. Jose, "Copper-oxide spinel absorber coatings for high-temperature concentrated solar power systems," *Solar Energy Materials and Solar Cells*, vol. 182, pp. 321–330, Aug. 2018, doi: 10.1016/j.solmat.2018.03.025.

[9] P. Ma, Q. Geng, X. Gao, T. Zhou, S. Yang, and G. Liu, "Aqueous solution-derived CuMn2O4 ceramic films for spectrally selective solar absorbers," *Ceram Int*, vol. 42, no. 16, pp. 19047–19057, Dec. 2016, doi: 10.1016/j.ceramint.2016.09.062.

[10] R. Bayón, G. San Vicente, C. Maffiotte, and Á. Morales, "Preparation of selective absorbers based on CuMn spinels by dip-coating method," *Renew Energy*, vol. 33, no. 2, pp. 348–353, Feb. 2008, doi: 10.1016/j.renene.2007.05.017.

[11] P. Ma, Q. Geng, X. Gao, S. Yang, and G. Liu, "Aqueous chemical solution deposition of spinel Cu1.5Mn1.5O4 single layer films for solar selective absorber," *RSC Adv*, vol. 6, no. 60, pp. 54820–54829, 2016, doi: 10.1039/c6ra08777a.

[12] V. Amrutha, S. Latha, P. Bera, S. John, G. Srinivas, and H. C. Barshilia, "Thermal treatment of stainless steel substrates along with a thin silicon layer for high temperature solar thermal applications," *Solar Energy*, vol. 262, Sep. 2023, doi: 10.1016/j.solener.2023.05.045.

[13] S. A. Abdullahi *et al.*, "Investigation of the Thermal Stability of a Solar Absorber Processed through a Hydrothermal Technique," *Solar*, vol. 2, no. 4, pp. 414–431, Dec. 2022, doi: 10.3390/solar2040025.

[14] O. F. Can, N. Celik, F. Ozgen, C. Kistak, and A. Taskiran, "Experimental and Numerical Analysis of the Solar Collector with Stainless Steel Scourers Added to the Absorber Surface," *Applied Sciences (Switzerland)*, vol. 14, no. 6, Mar. 2024, doi: 10.3390/app14062629.

[15] V. Pelenovich *et al.*, "AlCrO protected textured stainless-steel surface for high temperature solar selective absorber applications," *Surf Coat Technol*, vol. 436, Apr. 2022, doi: 10.1016/j.surfcoat.2022.128282.

[16] M. Joly *et al.*, "Optical and structural analysis of sol–gel derived Cu–Co–Mn–Si oxides for black selective solar nanocomposite multilayered coatings," *Solar Energy Materials and Solar Cells*, vol. 143, pp. 573–580, Dec. 2015, doi: 10.1016/j.solmat.2015.06.058.

[17] T. Boström, S. Valizadeh, J. Lu, J. Jensen, G. Westin, and E. Wäckelgård, "Structure and morphology of nickel-alumina/silica solar thermal selective absorbers," *J Non Cryst Solids*, vol. 357, no. 5, pp. 1370–1375, Mar. 2011, doi: 10.1016/j.jnoncrysol.2010.09.023.

[18] L. Noč and I. Jerman, "Review of the spectrally selective (CSP) absorber coatings, suitable for use in SHIP," May 01, 2022, *Elsevier B.V.* doi: 10.1016/j.solmat.2022.111625.

[19] K. Xu, M. Du, L. Hao, J. Mi, Q. Yu, and S. Li, "A review of high-temperature selective absorbing coatings for solar thermal applications," Mar. 01, 2020, *Chinese Ceramic Society*. doi: 10.1016/j.jmat.2019.12.012.

[20] Y. Chen *et al.*, "Colored and paintable bilayer coatings with high solar-infrared reflectance for efficient cooling," 2020.

[21] C. , J. and G. W. S. Brinker, "Sol-gel science: the physics and chemistry of sol-gel processing.," *Academic press*, 2013.

[22] L. Kaluža, K. Kaluža, A. Angelaˇangelašurca-Vuk, B. Orel, and J. Stefan, "Structural and IR Spectroscopic Analysis of Sol-Gel Processed CuFeMnO 4 Spinel and CuFeMnO 4 /Silica Films for Solar Absorbers GORAN DRAŽIČDRAˇDRAŽIDRAŽIˇDRAŽIČ AND PRIMOŽPRIMOˇPRIMOŽ PELICON," 2001.

[23] A. Schüler *et al.*, "On the feasibility of colored glazed thermal solar collectors based on thin film interference filters," in *Solar Energy Materials and Solar Cells*, Oct. 2004, pp. 241–254. doi: 10.1016/j.solmat.2004.02.045.

[24] A. Schüler *et al.*, "Sol-gel deposition and optical characterization of multilayered SiO2/Ti1-xSixO2 coatings on solar collector glasses," *Solar Energy Materials and Solar Cells*, vol. 90, no. 17, pp. 2894–2907, Nov. 2006, doi: 10.1016/j.solmat.2006.05.003.

[25] E. C. Zimmermann and A. Dalcher, "Incoherent radiative properties of an opaque body," 1991. doi: 10.1364/OA_License_v1#VOR.

[26] H. G. Tompkins and E. A. Irene, *Handbook of Ellipsometry*. Elsevier Inc., 2005. doi: 10.1515/arh-2005-0022.
[27] H. Fujiwara, *Spectroscopic Ellipsometry*. Wiley, 2007. doi: 10.1002/9780470060193.
[28] H. G. Tompkins, J. H. Baker, S. Smith, and D. Convey, “Spectroscopic Ellipsometry and Reflectometry: A User’s Perspective.”
[29] C. F. Bohren and D. R. Huffman, *Absorption and Scattering of Light by Small Particles*. Wiley, 1998. doi: 10.1002/9783527618156.
[30] D. V. Likhachev, N. Malkova, and L. Poslavsky, “Modified Tauc-Lorentz dispersion model leading to a more accurate representation of absorption features below the bandgap,” *Thin Solid Films*, vol. 589, pp. 844–851, Aug. 2015, doi: 10.1016/j.tsf.2015.07.035.